SolarPACES 2022, 28th International Conference on Concentrating Solar Power and Chemical Energy Systems
Emerging and Disruptive Concepts
https://doi.org/10.52825/solarpaces.v1i.699
© Authors. This work is licensed under a Creative Commons Attribution 4.0 International License
Published: 07 Feb. 2024

An Integrated Light Pipe Receiver and Thermal Energy Storage

Christi Madsen[1][https://orcid.org/0000-0003-1391-420X]

[1] Texas A&M University, USA and Sunstrike Optics LLC, USA

Abstract. An integrated light pipe receiver and thermal energy storage (TES) architecture is proposed for solar process heat applications. Simulations demonstrate the benefits of increased heat transfer area to a low conductivity TES medium and reduced surface radiation losses. When compared against a baseline design with a hemispherical absorber, the integrated light pipe receiver enables up to a factor of three higher energy storage for distributed absorption relative to localized absorption at the top of the TES. For a lower thermal conductivity TES medium or baselining to a flat-top absorber, an increase in thermal energy storage up to a factor of five results.

Keywords: Solar concentrator, Light pipe, Thermal energy storage, Solar furnace.

1. Introduction

Solar-to-thermal energy conversion is typically implemented by an absorber within a receiver followed by a heat transfer medium which is coupled to a thermal energy storage (TES) system. For a given system, an optimum concentration exists above which the thermal losses degrade the efficiency, dominated by radiative losses. To overcome the substantial thermal losses as the receiver temperature T_R increases, cavity receivers [1] have been demonstrated that limit the receiver aperture, and thus the area over which radiative and convective losses occur. Volume absorbers have also been investigated that combine the receiver absorbing function and TES simultaneously [2]. Studies have reported the use of soda lime glass [3], [4] for absorption and storage up to 1300°C. While cavity receivers and volume absorbers have been explored, improvements in the receiver-to-TES efficiency at high concentrations and temperatures are needed. This paper focuses on the receiver-to-TES design by proposing a novel light pipe integrated receiver and providing initial simulations to demonstrate its benefits for solar process heat applications and solar furnaces.

2. Glass Light Pipes and Geometric Concentration Limits

Glass light pipes are proposed for transmitting and distributing solar energy from the receive aperture to an absorber and TES material. While volume absorption in borosilicate and soda lime glasses may be used to convert the solar energy to heat along the light pipe, we are also interested in low absorption glass for transmitting the light to an absorber, whether it be a surface or volume type, embedded in the TES medium. While fused silica and quartz are more expensive, they offer the advantage of very low loss across the solar spectrum and the ability to operate at high temperatures, up to 1200C.

A silica glass light pipe is capable of guiding concentrated sunlight with high transmission efficiency over meter-scale distances compatible with TES dimensions. The etendue limit imposed by the limited numerical aperture, assuming air cladding of the glass light pipe, allows very high concentrations for direct normal irradiance (DNI) solar, in theory > 10,000x. In practice, tracking tolerances and surface roughness considerations are limiting factors. Geometric concentrations (i.e. input area divided by output area) on the order of 2,000x, and potentially higher, are achievable with commercial tracking systems, particularly ones developed for concentrating photovoltic systems. Thus, a one inch (25.4 mm) diameter silica glass pipe would efficiently transmit the concentrated power from a one square meter (mirror or lens) input. Given the expense of fused silica, borosilicate glass offers economic advantages and reasonable transmission, i.e. the absorption is not a limiting factor for meter-scale lengths. In the following, we focus on the location of the light absorption, assuming a blackbody surface absorber, within the TES to understand the potential benefits.

3. Localized Flat-Top Receiver-TES

To establish a baseline for design comparisons, a representative optical concentrating path composed of a lens followed by a secondary concentrator and a basic receiver with a limited aperture and a flat blackbody absorbing surface as shown in Figure 1a are chosen as a baseline design. Simulations using COMSOL Multiphysics software were done, starting with ray tracing of the light path. A direct normal irradiance (DNI) of 950W/m2 was assumed for 7 hours a day. A spherical lens with 1m diameter, 1.7m focal length, and 90% clear aperture was used to simulate the primary concentrator.

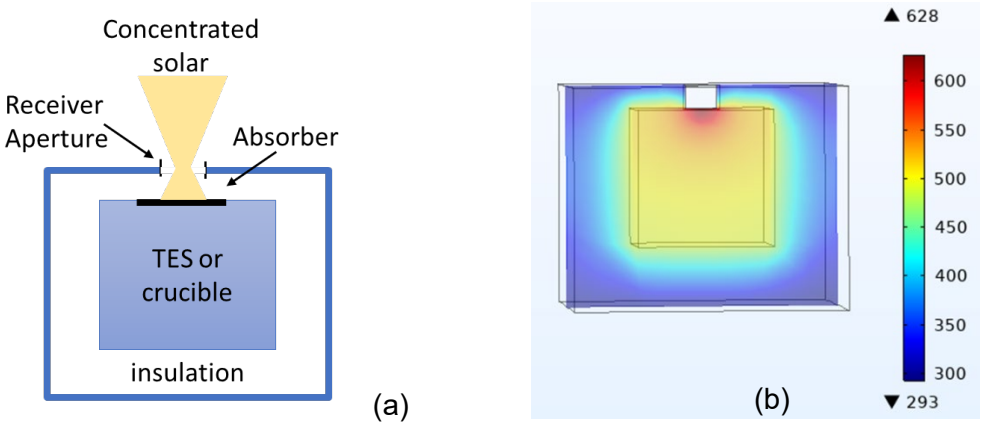

Figure 1. a) Basic TES structure with a localized, flat-top receiver. b) COMSOL Multiphysics heat transfer simulation showing temperature (K) distribution after 7 hours of charging.

For simulations, an iron cube (0.2m on a side) is first chosen as the TES material and fire brick (with a minimum 0.1m thickness) is chosen as the insulation material. A ray trace simulation provides the absorbed power distribution on the blackbody receiver surface for a coupled heat transfer simulation to determine the temperature distribution after 7 hours of solar charging from an ambient temperature of 20°C. Including surface-to-ambient radiation, the simulated results for the baseline case are shown in Figure 1b.

4. Light Pipes for Beam Delivery

A remoted receiver-TES is shown in Figure 2a with a glass light pipe that the concentrated solar is coupled into for low loss delivery to the absorbing surface. The glass was assumed to have negligible absorption. A COMSOL Multiphysics heat transfer simulation is shown with the same input solar energy as in the baseline case. A ray trace example, assuming normal incidence and a wavelength of 550nm, is shown in Figure 3a for coupling into a glass slab light pipe with a thickness of 1cm, width of 8cm and length of 20cm. The achievable temperature

increase above ambient for the TES is a factor of 2 greater for the light pipe integrated design over the baseline as shown in Figure 3b.

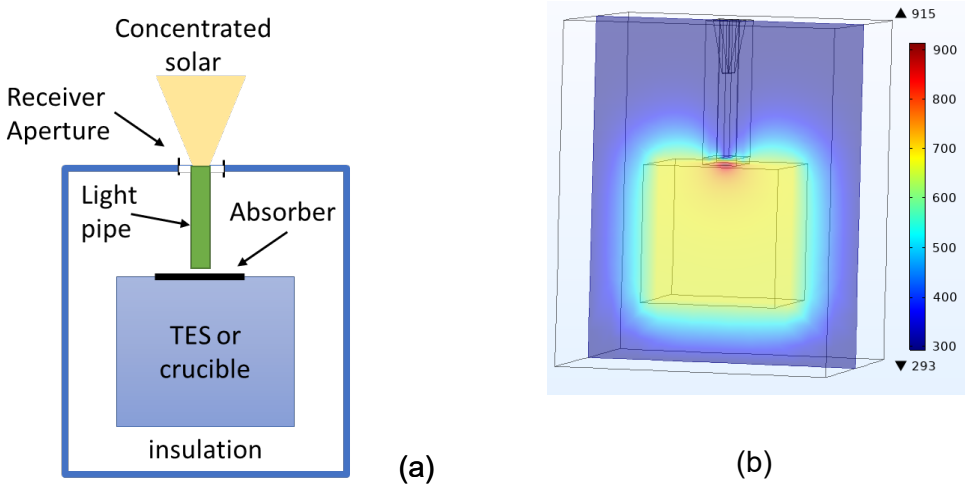

Figure 2. a) A light pipe integrated receiver and b) COMSOL thermal simulation showing the temperature distribution.

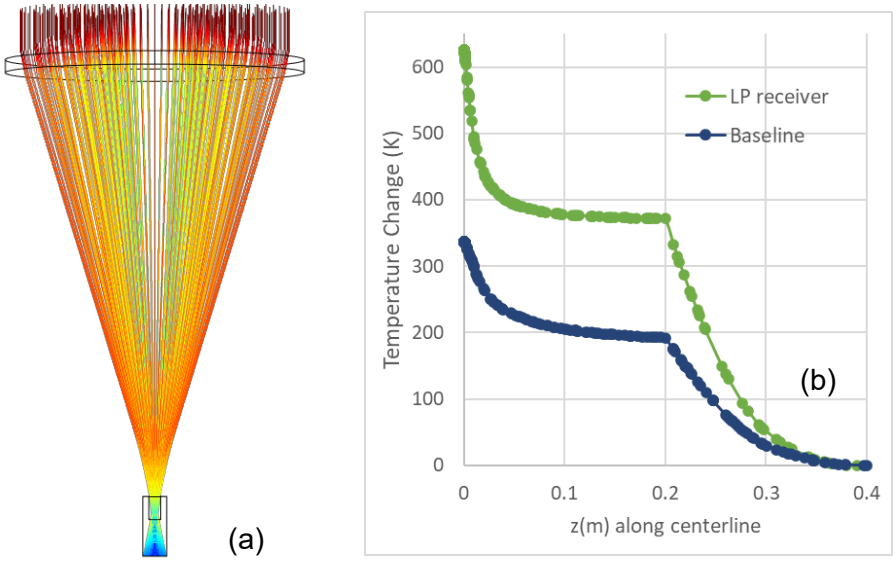

Figure 3. a) Ray trace simulation for coupling into the light pipe from a lens. b) Change in temperature down the receiver-storage centerline after 7 hours on-sun for the proposed and baseline design.

Besides providing a low loss transmission path between the concentrated input plane and absorber surface, a leaky light pipe can distribute the light onto a larger absorber surface. The slab geometry shown in Figure **4** was considered first. The tapering of the secondary concentrator and leaky light pipe are in one dimension. A ray trace is shown from a sideview as well as a closeup of the leaky slab region in a rotated view in Figure **4**. The absorbing surface is where the rays terminate.

The asymmetric nature of light distribution for the slab requires a unique secondary concentrator with a 1D taper to guide the light along the slab thickness dimension but allow it to expand to the full width dimension of the slab. A simpler concentrating geometry may be used for an axisymmetric case whereby the light is distributed along the surface of a cylinder. From a heat transfer perspective from the absorber to the surrounding TES material, we compare the basic heat conduction equations for a slab and cylinder. If the TES height, volume and absorbing areas are the same between the slab and cylinder geometries, the cylinder is

advantageous for ratios of the cylinder outer to inner radius of 2 or more. Thus, we continue with the axisymmetric geometry for thermal simulations.

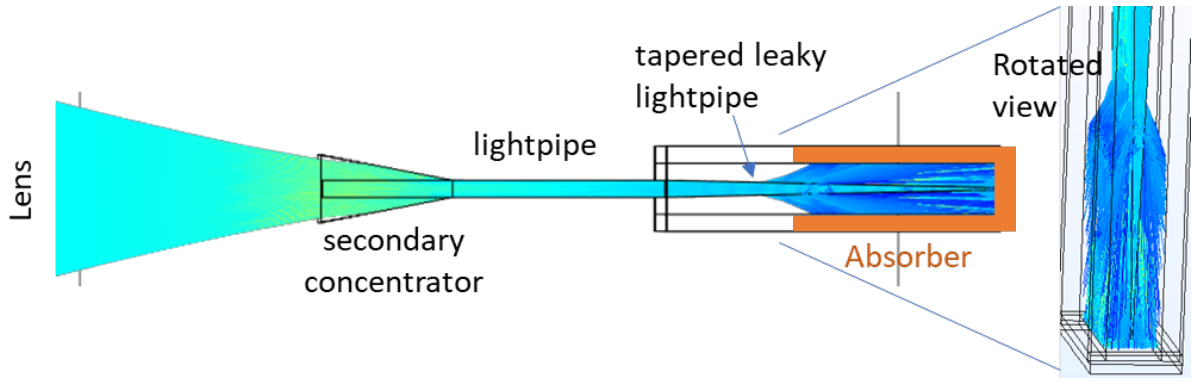

Figure 4. Sideview of ray trace from a lens to a secondary concentrator that is coupled to a lightpipe. A tapered lightpipe disperses the light to an absorber along the slab walls and bottom.

5. Distributed Axisymmetric Heating Simulations

The next step is to embed the light pipe and absorber in the TES to illuminate a larger area that is thermally coupled to the TES than is achievable with localized top-surface heating. Low-cost solid particles, such as rocks and recycled glass, are being explored for TES; however, their conductivity is relatively low. To evaluate heat transfer with a lower conductivity material, we chose a conductivity of 2 W/m-K [5]. An example structure is shown in Figure **5**a and b, consisting of a steel (or iron) cylinder that absorbs the solar radiation at the edges of the glass light pipe. The outer TES cylinder radius is 16cm and height is 25cm. The inner radius for the absorber is 4cm. An insulation thickness of 5cm was used on all sides and top, and 10cm on the bottom. The ambient temperature was set to 25C. A localized heating configuration is shown in Figure **5**c and d for comparison. A transparent, 3mm-thick glass cover is used for both configurations which prevents particles from getting into the cavity. The TES volume is V=0.022m^3, and the absorber area is 0.066m^2.

A uniform heat source is simulated on the absorber, having good thermal conductivity and representing the absorption of incident solar radiation carried by the light pipe. A gap separates the light pipe from the glass cover to reduce convective losses. A physics-controlled fine mesh is used for the simulations. The material properties used in the simulations are summarized in Table 1 and were assumed to be constant over the simulated temperature range. Insulator properties that are characteristic of ceramic wool are used while the properties of iron are assumed for the absorber. The TES properties are based on soda-lime glass with a slightly high average thermal conductivity used since radiative conductivity was not incorporated. In future simulations, temperature-dependent thermal properties and radiative conductivity for the glass will be incorporated.

Table 1. Material thermal properties for simulations: conductivity, specific heat, and density.

Material	k(W/m-K)	C_p(J/kg-K)	ρ(kg/m^3)
TES	2	2500	870
Absorber	55	456	7920
Insulator	0.04	840	20

Simulations for the TES are shown in Figure **6**a for a 5-hour charging period with 1000W incident on the absorber and a subsequent 5 hour discharging period in Figure **6**b. The top graphs show the average, minimum, and maximum temperatures for the TES. The middle graphs show the stored thermal energy, including the TES, absorber and light pipe. The lower graphs show the net thermal loss (W), dominated by radiative losses and natural convection from the

top and sides. The average TES temperature after 5 hours was 587K, for a total energy storage of 4.7kWh.

For comparison, a charging cycle simulation for localized heating is shown in Figure **7**, using the same TES cylinder dimensions and insulation as above. The convective loss surface areas and natural convection conditions are the same as for the distributed heating case. The TES volume is V=0.020 m^3, and the absorber area is 0.010 m^2. Notably, the maximum temperature is substantially higher than for the distributed case, and subsequently, the radiative losses are much higher. After 5 hours of charging, the maximum TES temperature is 1159K and the net thermal loss is 600W, versus a maximum temperature of 821K for the distributed heating case and a net loss less than 200W. The maximum energy storage was 2.77kWh, only 59% of the distributed storage case.

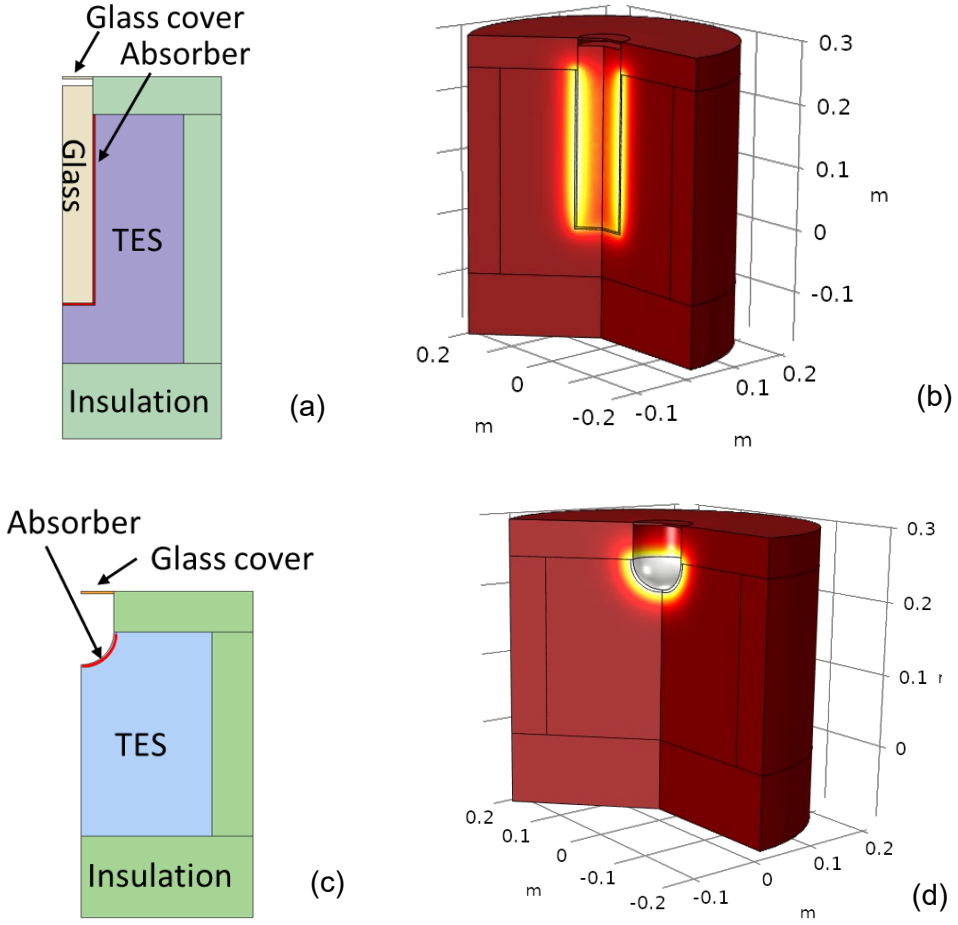

Figure 5. Cylinder a) cross-section and b) rotational views for a distributed absorber and similarly in c) and d) for a localized absorber. For b) and d), the absorber is shown in white and the color variation indicates the temperature rise at the start of the charging period.

During charging, the net loss is substantially greater for localized heating than for the distributed heating. If the incident solar radiation is increased to 2kW, the distributed heating case performs even more favorably, storing 2.4 times as much energy relative to the localized heating case. For discharging, the radiative losses change quickly, so the remaining convective losses dominate in both the localized and distributed heating cases.

Figure **8** compares the simulation results between the distributed and localized heating configurations over a range of input powers to the absorber from 1kW to 3kW, after 5 hours charging time. The input power is after any losses in the concentrating optical path. The material properties were assumed to be constant with temperature, which will need to be modified in future work, as referenced in [6] and [7]. The same natural convectiion losses were

assumed for all sides, so the difference in results is due predominantly to the radiative losses. The surface emissivity of glass and the absorber were taken to be 0.93 and 0.9, respectively. The average TES temperatures are shown in Figure **8**a. The distributed absorber was able to achieve a higher average TES temperature and a factor of 1.7 to 3 times more thermal energy storage as shown in Figure **8**b over the localized heating. The efficiency was calculated as the ratio of the stored thermal energy to incident solar energy and is shown in Figure **8**c. It indicates that the distributed case will scale more efficiently with input energy than the localized case.

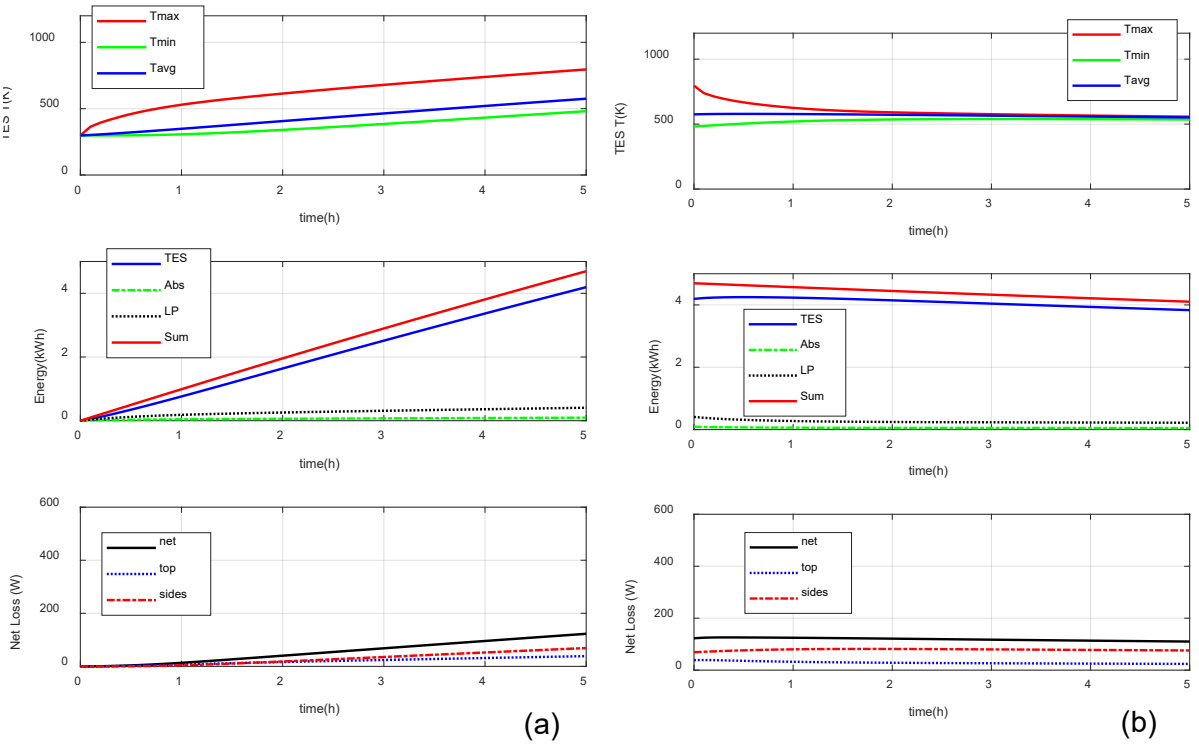

Figure 6. Distributed heating for P_{abs}=1kW: a) charging and b) discharging.

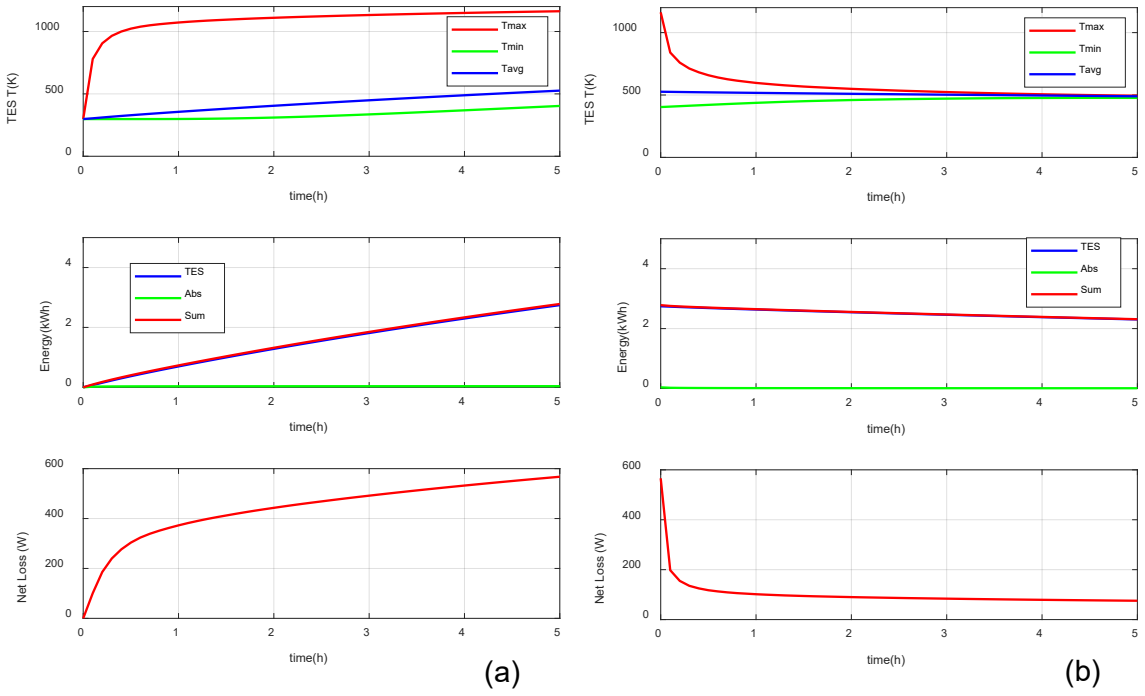

Figure 7. Localized heating simulations for Pabs=1kW: a) charging and b) discharging.

To simulate the impact of a TES medium with a lower thermal conductivity, the simulation was repeated for the TES material with a conductivity of 1 W/m-K (instead of 2 W/m-K). Figure **8**b shows the stored energy results in dashed lines. Because the thermal energy is not transferred as efficiently, the localized heating case has a substantially reduced energy storage while the distributed heating case showed only a minor difference. For the lower TES conductivity case, the impact of distributed heating improves the energy storage by a factor of 2.5 to 4.8 over the localized heating case, depending on the absorbed power.

A flat-top absorber has more radiation loss than the hemispherical absorption surface assumed for the baseline case as shown in Figure **8**b assuming a glass conductivity k=2 W/m-K. The ratio of energy stored for the distributed case relative to a flat-top localized absorber is 2.7 to 5.1.

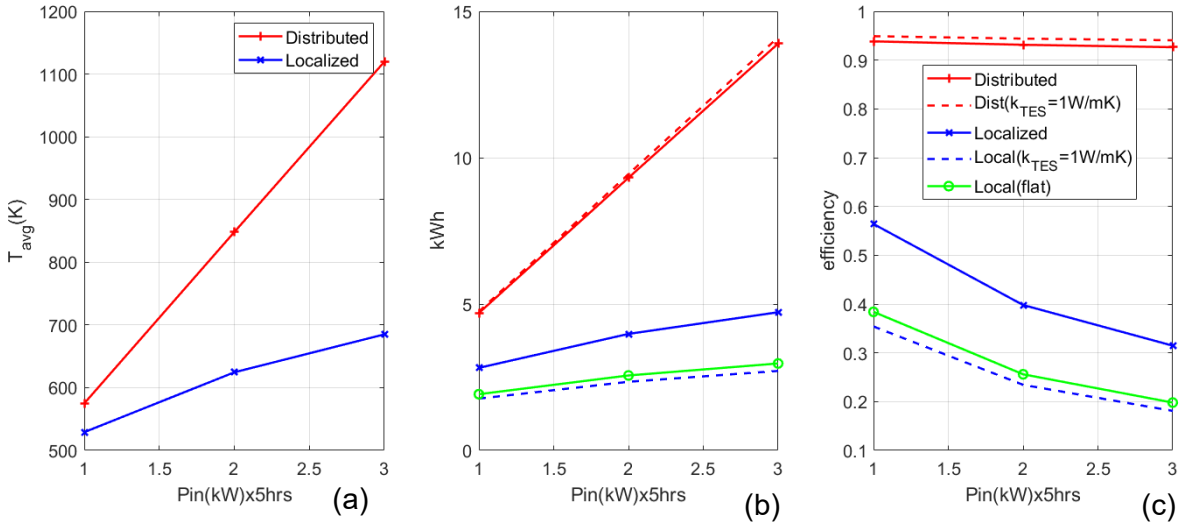

Figure 8. Comparison of distributed (red) and localized (blue) heating simulations after 5 hours versus absorbed power P_{in}. a) Average TES temperatures, b) thermal energy storage (kWh) and c) efficiency. The same legend applies for b) and c).

6. Summary

An approach based on a light pipe integrated receiver-TES for distributing the absorbed solar energy has been simulated, demonstrating that it can effectively improve the stored thermal energy versus localized absorption at the top surface of the TES. For future work, temperature-dependent material properties and radiative conductivity for glass will be incorporated as well as a more detailed optical path analysis including glass absorption. Further improvements can be made in minimizing thermal losses, especially for the discharge phase. As an example, reported measurements on a TES at a temperature of 800°C with dimensions of 3m x 3m x 3m for falling-particle receives [8] has achieved 4.4% steady-state heat loss over a 24 hour period.

Competing interests

The author declares no competing interests.

Author contributions

Christi Madsen: conceptualization, simulations, writing.

Data availability statement

The data is based on simulations using commercial software which can be replicated using the simulation inputs defined in the paper.

References

1. W. T. Xie, Y. J. Dai, and R. Z. Wang, “Numerical and experimental analysis of a point focus solar collector using high concentration imaging PMMA Fresnel lens,” Energy Conversion and Management, vol. 52, no. 6, pp. 2417–2426, Jun. 2011, doi: 10.1016/j.enconman.2010.12.048.
2. A. H. Slocum et al., “Concentrated solar power on demand,” Solar Energy, vol. 85, no. 7, pp. 1519–1529, Jul. 2011, doi: 10.1016/j.solener.2011.04.010.
3. B. Elkin, L. Finkelstein, T. Dyer, and J. Raade, “Molten Oxide Glass Materials for Thermal Energy Storage,” Energy Procedia, vol. 49, pp. 772–779, Jan. 2014, doi: 10.1016/j.egypro.2014.03.083.
4. E. Casati, A. Lankhorst, U. Desideri, and A. Steinfeld, “A co-located solar receiver and thermal storage concept using silicate glass at 1000°C and above: Experiments and modeling in the optically-thick regime,” Solar Energy, vol. 177, pp. 553–560, Jan. 2019, doi: 10.1016/j.solener.2018.11.052.
5. G. Zanganeh, A. Pedretti, S. Zavattoni, M. Barbato, and A. Steinfeld, “Packed-bed thermal storage for concentrated solar power – Pilot-scale demonstration and industrial-scale design,” Solar Energy, vol. 86, no. 10, pp. 3084–3098, Oct. 2012, doi: 10.1016/j.solener.2012.07.019.
6. S. Yang, J. Wang, P. D. Lund, C. Jiang, and X. Li, “High performance integrated receiver-storage system for concentrating solar power beam-down system,” Solar Energy, vol. 187, pp. 85–94, Jul. 2019, doi: 10.1016/j.solener.2019.05.041.
7. A. El-Leathy et al., “Thermal performance evaluation of lining materials used in thermal energy storage for a falling particle receiver based CSP system,” Solar Energy, vol. 178, pp. 268–277, Jan. 2019, doi: 10.1016/j.solener.2018.12.047.
8. C. Ho et al., “Technology Advancements for Next Generation Falling Particle Receivers,” Energy Procedia, vol. 49, pp. 398–407, Jan. 2014, doi: 10.1016/j.egypro.2014.03.043.